Applied Catalysis B: Environmental 115–116 (2012) 245–252

Contents lists available at SciVerse ScienceDirect

Applied Catalysis B: Environmental

journal homepage: www.elsevier.com/locate/apcatb

One-pot pyridine-assisted synthesis of visible-light-driven photocatalyst Ag/Ag_3PO_4

Yongping Liu[b,c], Liang Fang[a,b,*], Huidan Lu[c,**], Yanwei Li[c], Changzheng Hu[a], Huogen Yu[d]

[a] Key Lab. of Nonferrous Materials and New Processing Technology, Ministry of Education, Guilin University of Technology, Guilin 541004, PR China
[b] School of Chemistry and Chemical Engineering, Guangxi University, Nanning, Guangxi, 530004, PR China
[c] College of Chemistry and Bioengineering, Guilin University of Technology, Guilin 541004, PR China
[d] Department of Chemistry, School of Science Wuhan University of Technology, Wuhan 430070, PR China

ARTICLE INFO

Article history:
Received 25 October 2011
Received in revised form
20 December 2011
Accepted 23 December 2011
Available online 31 December 2011

Keywords:
Plasmonic
Photocatalytic
Silver orthophosphate
Hydrothermal
Pyridine

ABSTRACT

A highly efficient and stable Ag/Ag_3PO_4 photocatalyst was prepared by a facile one-pot hydrothermal method assisted by pyridine. Pyridine played two important roles in the synthesis: it could work as a coordination agent role of Ag^+ and act as reductant for reduce partial Ag^+ to metallic Ag. The influences of pyridine amount, reaction temperature and pH value on the content of Ag in the composite were investigated. The diffuse reflectance spectra (DRS) indicated that the Ag/Ag_3PO_4 had strong absorption in UV and visible light regions. The photocatalytic activity of the composite was evaluated by the degradation of methyl orange (MO) and phenol under visible light irradiation. The experimental results indicated that the Ag/Ag_3PO_4 showed highly efficient and stable photocatalytic activity under visible light irradiation. It was considered that the excellent performance resulted from the surface plasmon resonance of Ag nanoparticles and a large negative charge of PO_4^{3-} ion.

1. Introduction

Heterogeneous photocatalysis using semiconductors has been considered as a cost-effective alternative for the destruction of persistent toxic organic compounds. Much research has been devoted to searching for active semiconductor photocatalysts that can degrade environmental pollutants under sunlight irradiation. TiO_2 [1–3] has been widely used as a photocatalyst because of its high activation, long-term stability, low price, and availability, but its band gap is too wide to absorb sunlight efficiently. In the recent years, a growing interest was also focused on the non-TiO_2-based photocatalyst, such as $PbBi_2Nb_2O_9$ [4], $BiVO_4$ [5], Bi_2WO_6 [6], $Zn_xCd_{1-x}S$ [7], $SrTiO_3$ [8] and so on. However, the above investigations about photocatalysts are mostly focused on the metal oxides or composite metal oxides. It is very necessary and important to develop new and highly efficient visible-light-driven photocatalysts.

More recently, Ye and co-workers [9] reported the new use of Ag_3PO_4 semiconductor in photocatalytic applications, where it exhibits extremely high photooxidative capabilities for the O_2 evolution from water and the decomposition of organic dyes under visible-light irradiation. More specifically, this novel photocatalyst can achieve a quantum efficiency of up to 90% at wavelengths greater than 420 nm, which is significantly higher than the previous reported values. They further investigated the s effects of shape and facet on the photocatalytic properties and found that Ag_3PO_4 rhombic dodecahedrons exhibit much higher activities than cubes for the degradation of organic contaminants, which is ascribed to the higher surface energy of {1 1 0} facets ($1.31\ J/m^2$) than that of {1 0 0} facets ($1.12\ J/m^2$)[10]. Zhu and co-workers. investigated the origin of photocatalytic activation of Ag_3PO_4 using first-principle density functional theory incorporating the LDA + U formalism. They found that Ag_3PO_4 had a large dispersion of conduction band and the inductive effect of PO_4^{3-}, which helped the separation of electron–hole pairs. It was demonstrated theoretically that the Ag vacancies with a high concentration in Ag_3PO_4 have a significant effect on the separation of electron–hole pairs and optical absorbance in the visible-light region [11]. The electrode potential of $Ag–Ag_3PO_4$ (0.45 V *vs.* NHE) is higher than that of $H_2–H^+$ [12], which means that Ag_3PO_4 is easier to be reduced to Ag^0 ($Ag_3PO_4 + 3e \rightarrow Ag^0 + PO_4^{3-}$) than H^+ ($2H^+ + 2e \rightarrow H_2$) under light irradiation in water. A silver orthophosphate grain absorbs

* Corresponding author at: Key Lab. of Nonferrous Materials and New Processing Technology, Ministry of Education, Guilin University of Technology, Guilin 541004, PR China. Tel.: +86 773 5896290; fax: +86 773 5896436.
** Corresponding author.
E-mail addresses: fanglianggl@yahoo.cn (L. Fang), lhuidan@yahoo.com.cn (H. Lu).

0926-3373/$ – see front matter © 2011 Elsevier B.V. All rights reserved.
doi:10.1016/j.apcatb.2011.12.038

a photon to generate an electron and a hole, and then the electron combines with an interstitial silver ion to give a silver atom. Therefore, it is a highly crucial task to improve the photocatalytic stability of Ag_3PO_4 while maintaining its high photocatalytic activity.

There have been some reports that the localized surface plasmon resonance (LSPR) [13–15] of noble-metal nanoparticles on photocatalyst can improve the photocatalytic activity and stability. Ag/silver halide structures have been developed as visible-light photocatalyst, such as Ag@AgCl [14,16–19], Ag@AgBr [20,21], and Ag@AgI [22]. It was found that the high catalyst activity for dyes decomposition was maintained effectively after successive cycling runs without the destruction of AgCl (Br, I) and the Ag^0 species formed during synthesis and irradiation processes could scavenge the positive holes (h^+) and then trap electrons to prevent the further decomposition of AgCl (Br, I). Ag/silver halide structures also have been used as co-catalysts to enhance photocatalytic activity of semiconductors, such as $Ag/AgBr/TiO_2$ [23,24], $AgBr–Ag–Bi_2WO_6$ [25], $Ag@AgCl/TiO_2/SnO_2$ [26], $Ag–AgI/Al_2O_3$ [22], $Ag–AgI/Fe_3O_4@SiO_2$ [27].

In this work, we have prepared Ag/Ag_3PO_4 photocatalyst to improve the stability of Ag_3PO_4. Since the LSPR absorption of silver nanoparticles lies in the visible region, the reducibility of Ag^+ ions of the Ag_3PO_4 lattice decrease significantly when the surface of Ag_3PO_4 is covered by Ag^0 nanoparticles. Furthermore, we designed a one-pot, novel and simple experimental approach to prepare the Ag/Ag_3PO_4 photocatalyst by a pyridine-assisted hydrothermal method. The pyridine (Py) which was introduced to the synthesis system, not only works as a coordination agent of Ag^+, but also as a reductant for reducing Ag^+ ions to metal Ag.

2. Experimental methods

2.1. Sample preparation

All the reagents were analytical grade and were obtained from Shanghai Reagents Company (Shanghai, China). Ag/Ag_3PO_4 composites were prepared by one step hydrothermal method with the contribution of pyridine. First, 0.6370 g of $AgNO_3$, appropriate amount of pyridine and 30 mL of distilled water were mixed together in a Teflon-lined stainless-steel autoclave with a volume capacity of 75 mL. Then 20 mL of $Na_3PO_4{\cdot}12H_2O$ solution (0.4752 g) was added with drop by drop to the above solution under vigorous stirring. After stirring for 30 min, the autoclave was sealed and maintained at 180 °C for 3 h, then cooled to room temperature naturally. The final products were collected by centrifugation, washed with distilled water and absolute ethanol several times and then dried in a vacuum at 70 °C for 8 h in the dark for further characterization. Ag/Ag_3PO_4 composites synthesized at 180 °C for 3 h with 1 mL, 2 mL and 3 mL of pyridine were marked as AAP-1, AAP-2 and AAP-3, respectively.

The Ag/AgBr (Ag/AgCl) reference photocatalyst was prepared as fellow: 0.6370 g of $AgNO_3$, 3 mL pyridine and 30 mL of distilled water were mixed together in a Teflon-lined stainless-steel autoclave with a volume capacity of 75 mL. Then 20 mL of solution with 0.3858 g NaBr (0.2191 g NaCl) was added with drop by drop to the autoclave under vigorous stirring and then adjust the pH of solution to 11.3 with the addition of 0.5 M NaOH drops. After 30 min, the autoclave was sealed and maintained at 180 °C for 3 h.

The N-doped TiO_2 reference photocatalyst was prepared by nitridation of commercially available TiO_2 powder (surface area 48 $m^2\,g^{-1}$) at 773 K for 10 h under NH_3 flow (flow rate of 350 mL min^{-1}).

2.2. Characterization

The microstructures of the as-prepared photocatalysts were characterized by scanning electron microscopy (SEM, JEOL JSM6380-LV) and transmission electron microscope (TEM, Tecnai G^2 F20, FEI). The crystal phases of Ag/Ag_3PO_4 composites were analyzed by PANalytical X'Pert PRO X-ray diffraction (XRD) with Cu Kα radiation (λ = 1.54 Å) in the range of 20–80°. The chemical compositions of the samples were determined by X-ray photoelectron spectroscopy (XPS, ESCALAB 250 with monochromatized Mg KR X-ray as the source). The resulting binding energies were calibrated to the C 1s (284.6 eV) peak. The diffuse reflectance spectra (DRS) were measured by a UV–vis spectrometer (UV-2450, Shimadzu) in the range of 200–800 nm. $BaSO_4$ was used as the reflectance standard material. The Brunauer–Emmett–Teller (BET) specific surface area of the sample was characterized by nitrogen adsorption with Quantachrome Nova 1200.

2.3. Photocatalytic activity

The photocatalytic activity of Ag/Ag_3PO_4 composite was evaluated by the degradation of two organic pollutants: MO and phenol. Experiments were carried out with 0.3 g Ag/Ag_3PO_4 powder synthesized at 180 °C for 3 h with 3 mL pyridine assisted suspended in a MO dye (phenol) solution (20 mg/L, 100 mL), which was prepared by dissolving the MO (phenol) in distilled water in a Pyrex glass cell. The optical system for the degradation reaction included a 450 W Xe lamp, a cutoff filter of 420 nm. Before illumination the suspension was magnetically stirred in the dark for 30 min to ensure the establishment of an adsorption/desorption equilibrium of dye on the sample surface. The experiments were carried out at room temperature in air. The suspension containing the sample powder and dye (phenol) was sampled every few minutes. The sample powder was then separated by centrifuging and the dye (phenol) solution was analyzed. The concentration of MO (phenol) was determined by monitoring the height of the maximum of the absorbance in ultraviolet-visible spectra (UV-2450, Shimadzu). The large absorbance at 463 nm for MO, or 270 nm for phenol was used to evaluate the variation of organic pollution concentration.

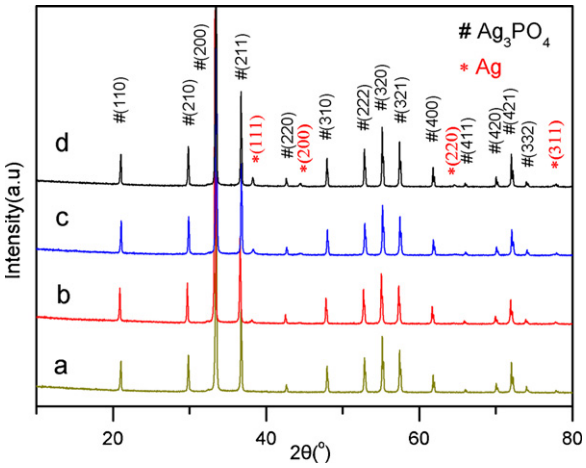

Fig. 1. XRD patterns of Ag/Ag_3PO_4 synthesized by the hydrothermal process at 180 °C for 3 h with a different addition of pyridine: (a) 0 mL, (b) 1 mL, (c) 2 mL and (d) 3 mL.

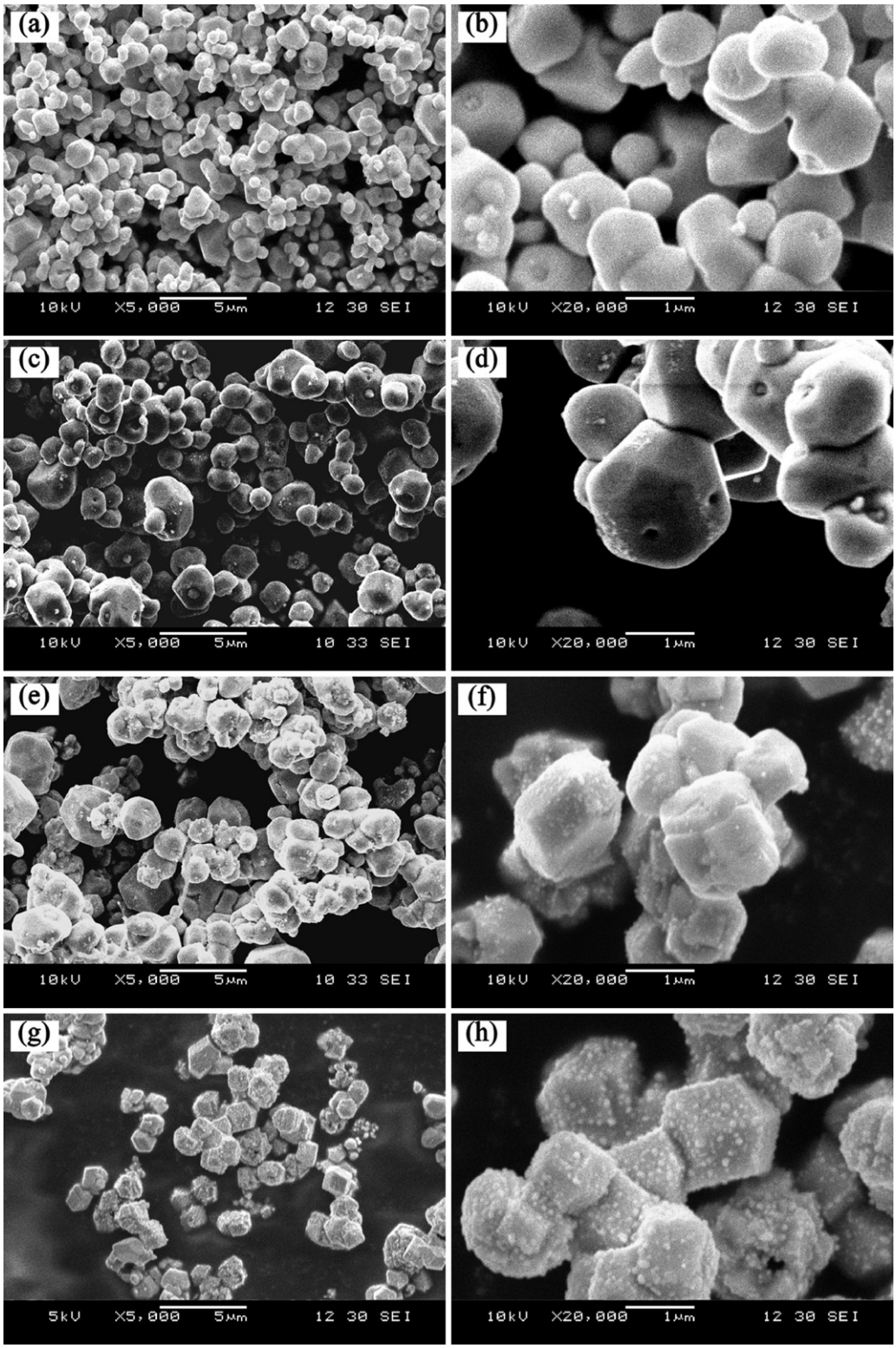

Fig. 2. SEM images of samples synthesized by the hydrothermal process at 180 °C for 3 h with a different addition of pyridine: (a, b) 0 mL, (c, d) 1 mL, (e, f) 2 mL, (g, h) 3 mL.

3. Results and discussion

3.1. Characterization of photocatalyst

Ag_3PO_4, a body-centred cubic structure with a lattice parameter of 6.004 Å [28], consists of isolated and regular PO_4 tetrahedral (P—O distance of ~1.539 Å) to form a body-centred cubic lattice and six Ag^+ ions are distributed among twelve sites of two-fold symmetry. XRD patterns of the sample (Fig. 1a) prepared by the hydrothermal method without the addition of pyridine confirm this crystal structure. All patterns match very well with the JPCDS (74-1876) standard data of Ag_3PO_4. When pyridine was added to the system, some new diffraction peaks at 38.1°, 44.3°, 64.2° and 77.5° appeared and their intensity increased with the amount of pyridine.

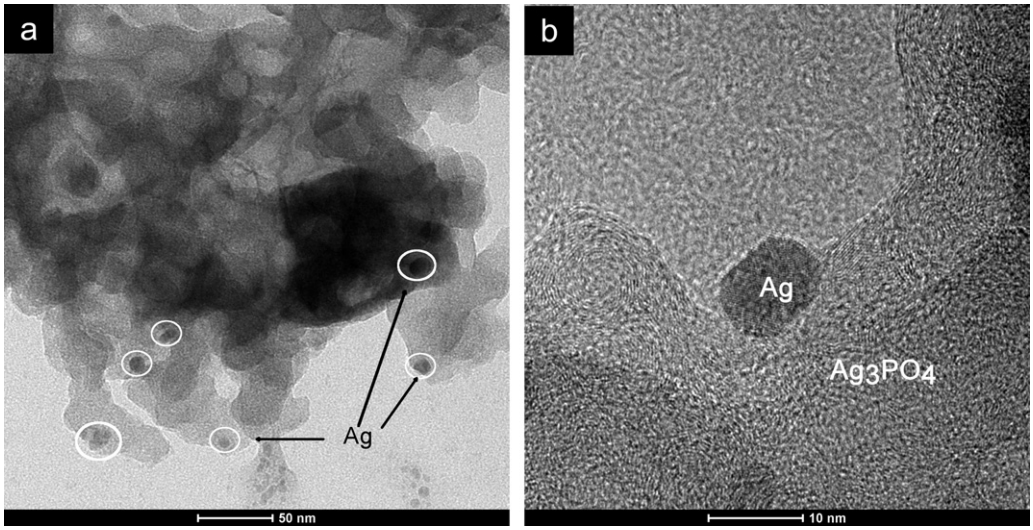

Fig. 3. TEM images of the Ag/Ag_3PO_4 sample synthesized by the hydrothermal process at 180 °C for 3 h with 3 mL pyridine.

The four diffraction peaks can be indexed into the (1 1 1), (2 0 0), (2 2 0), and (3 1 1) crystalline planes of metallic Ag (JCPDS file: 65-2871), respectively, which are marked with "*" in Fig. 1b–d. In addition, no other peaks of impurities or other phases such as Ag_xO are observed in XRD patterns of Ag/Ag_3PO_4 composites, indicating that the samples only contain the metallic Ag and Ag_3PO_4.

Fig. 2 shows the morphology of Ag/Ag_3PO_4 composites with a different addition of pyridine. With the addition of pyridine, the size of Ag_3PO_4 particles does not change obviously, and the estimated average diameter of the Ag_3PO_4 is between 0.3 and 1.5 μm. However, the morphology of Ag_3PO_4 particles changed regularly with increase in pyridine concentration. The Ag_3PO_4 particles synthesized without pyridine show spherical morphology (Fig. 2a and b). When pyridine was added to the reaction system, the corners and edges of Ag_3PO_4 particles are slightly clear and the tiny particles of Ag nanoparticles are clearly covering on the surface of the large Ag_3PO_4 particles. Moreover, the amount of Ag nanoparticles increases with the increasing concentration of pyridine. When the amount of pyridine increases to 3 mL, the obtained products are rhombic dodecahedral particles (Fig. 2g and h). The corresponding TEM images of the Ag/Ag_3PO_4 sample were shown in Fig. 3. It is clearly to observe that the Ag nanoparticles with a size of 5–20 nm are closely deposited to the surface of rhombic dodecahedral Ag_3PO_4. It could be concluded that the presence of pyridine played a key role in the formation of Ag/Ag_3PO_4 composite.

The XRD patterns and SEM images of Ag/Ag_3PO_4 composites prepared at different hydrothermal temperature are shown in Figs. 4 and 5, respectively. There are little of Ag nanoparticles appearing on the surface of the Ag_3PO_4 at 60 °C, indicating that a low temperature was not in favor of the reduction of Ag^+. With the increase in hydrothermal temperature, the content of Ag nanoparticles in composite increased while all samples still show a rhombic dodecahedral morphology (Fig. 5). Therefore, the above results demonstrated that the morphology of Ag_3PO_4 was mainly controlled by the pyridine while the amount of metallic Ag was determined by the hydrothermal temperature. Therefore, it is possible for us to prepare various rhombic dodecahedral Ag/Ag_3PO_4 photocatalysts with a controlled composition.

On the basis of the above experimental observations, we propose a possible formation mechanism for the formation of Ag/Ag_3PO_4 composites using hydrothermal method. The overall chemical reaction involved in the hydrothermal synthesis can be briefly described by Eqs. (1)–(2).

$$Ag^+ + nPy \rightarrow Ag^+(Py)_n \quad (n = 1, 2) \tag{1}$$

$$Ag^+(Py)_n + 2OH^- \rightarrow Ag + Py^+O^- + (n-1)Py + H_2O \tag{2}$$

Pyridine is a simple and fundamentally important heterocyclic aromatic organic compound. It is structurally related to benzene, wherein one CH group in the six-membered ring is replaced by a nitrogen atom. The nitrogen atom on pyridine features a basic lone pair of electrons. Because this lone pair is not delocalized into the aromatic-system, pyridine is basic with chemical properties similar to tertiary amines [29]. Pyridine itself is a relatively weak ligand in forming complexes with metal ions [30]. The formation of two types of complexes of different stoichiometric composition $Ag^+(Py)_2$ and $Ag^+(Py)$ is predominant in the Ag–pyridine system [31]. In reaction Eq. (1), the pyridinium cation of coordination between Ag^+ and pyridine can slow the concentration of free Ag^+ ions in reaction system. Therefore, it is possible for pyridine to rationally control the release rate of Ag^+ ions, which may result in the formation of Ag_3PO_4 with rhombic dodecahedral structures. In contrast, without the pyridine, the free Ag^+ ions with a higher concentration produce

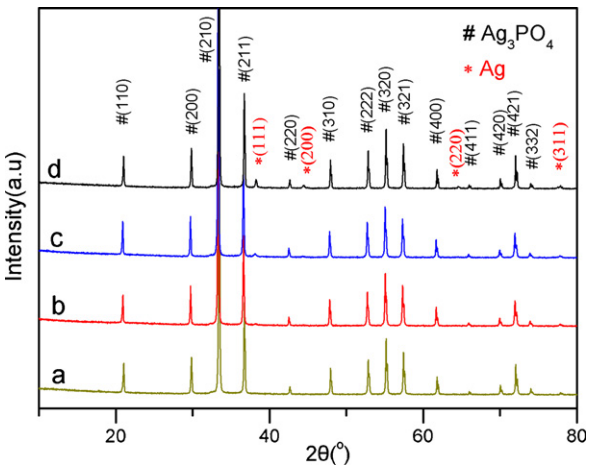

Fig. 4. XRD patterns of samples synthesized by the hydrothermal process at (a) 60 °C, (b) 100 °C, (c) 140 °C, (d) 180 °C with 3 mL pyridine for 3 h.

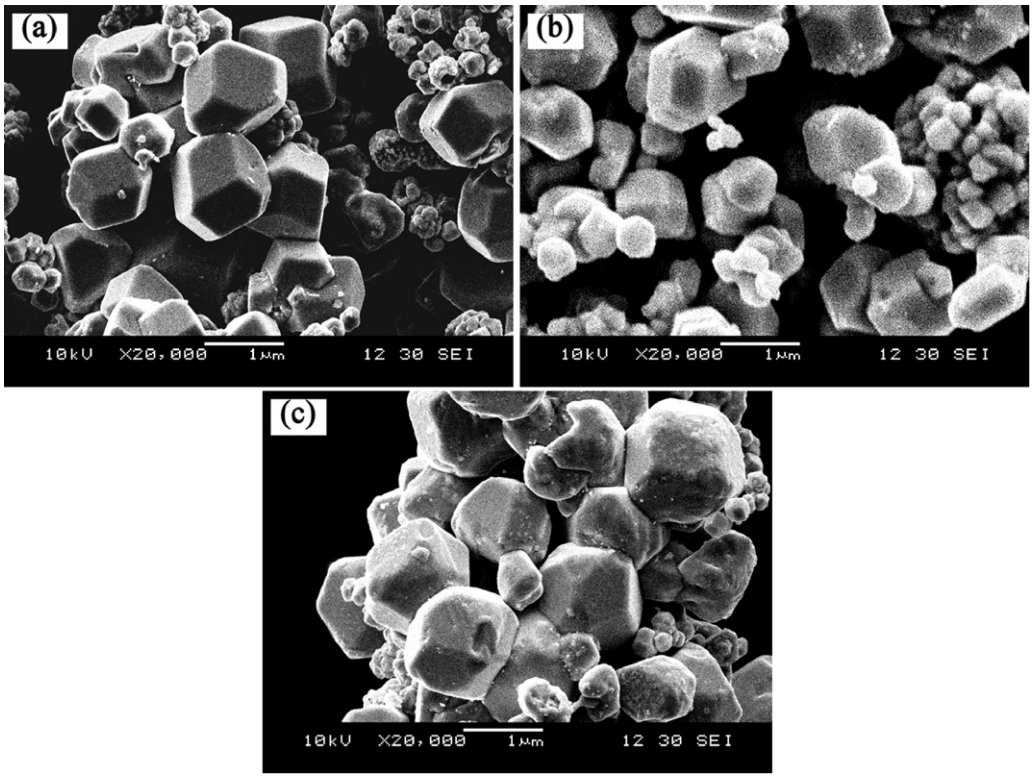

Fig. 5. SEM images of samples synthesized by the hydrothermal process at (a) 60 °C, (b) 100 °C, (c) 140 °C with 3 mL pyridine for 3 h.

a rapid nucleation and growth rates of Ag_3PO_4 crystals, leading to an irregularly spherical morphology. As a result, with the increase in pyridine concentration, Ag_3PO_4 crystals tend to have rhombic dodecahedral structures.

The above experiments result shows that the presence of pyridine is essential for the formation of Ag/Ag_3PO_4 composite in present reaction system. It could be considered that pyridine acted as a reducing reagent in the process of preparing Ag^0 in the Ag_3PO_4 structure. Furthermore, hydrothermal reaction temperature and pH are also important factors for determining the Ag^0 content on the Ag_3PO_4 surface. It has been found that high temperature was in favor of the Ag^+ reducing from Figs. 4 and 5. In order to study the influence of pH to Ag/Ag_3PO_4 composites, we substituted Na_2HPO_4 for Na_3PO_4 to react with $AgNO_3$ in hydrothermal system with 3 mL pyridine assisted. When Na_2HPO_4, $AgNO_3$ and pyridine were mixed in a solution before hydrothermal reaction, a translucent solution (pH 9.11) was obtained. However, when Na_3PO_4 was used as the precursor, a yellow colloid solution (pH 11.3) containing Ag_3PO_4 particles was obtained. It reveals that pyridine have relative a stronger coordinate ability with Ag^+ in a lower pH. After hydrothermal reaction in 180 °C for 3 h in Na_2HPO_4 system, only pure Ag_3PO_4 particles were received which means that no Ag^+ ions were reduced to metallic Ag. It can be deduced that pyridine has the reducing capacity only in a strong alkaline solution. Therefore, we proposed a formula on a reduction reaction of silver ions with pyridine, shown in Eq. (2). Pyridine possesses weak reducing capacity, and could partly reduce Ag^+ ions to Ag^0 in alkaline and high temperature.

On the basis of the above analysis, pyridine not only plays a coordination agent role for Ag^+, but also acts as a reducing reagent for reducing partial Ag^+ to metallic Ag during the one-pot hydrothermal synthesis.

The UV–vis diffuse reflectance spectra for the samples prepared at different pyridine addition are shown in Fig. 6. The strong absorption below a wave-length of 530 nm is associated with the optical band gap of Ag_3PO_4. The indirect band gap of Ag_3PO_4 is estimated to be 2.36 eV, as well as, direct transition is 2.43 eV [9]. In the case of the Ag/Ag_3PO_4 composite, the absorbance at the range of 500–800 nm is higher than that of pure Ag_3PO_4, which is attributed to the characteristic absorption of surface plasmon absorption of metallic silver on Ag_3PO_4 surface. The absorption intensity of the composites was increased with the increasing amount of pyridine in reaction system. This result is consistent with the former discovery that the amount of Ag nanoparticles on the surface of Ag_3PO_4 increases with the growth of amount of pyridine.

The elemental composition, chemical status, and silver content of Ag/Ag_3PO_4 composite were further analyzed by X-ray photoelectron spectroscopy (XPS). The XPS peaks of Ag 3d and P 2p are shown in Fig. 7. It is found that the peaks of Ag $3d_{5/2}$ and Ag $3d_{3/2}$ are located at ~368 and ~374 eV, respectively (Fig. 7a). The Ag $3d_{3/2}$ and Ag $3d_{5/2}$ peaks can be further divided into two different peaks

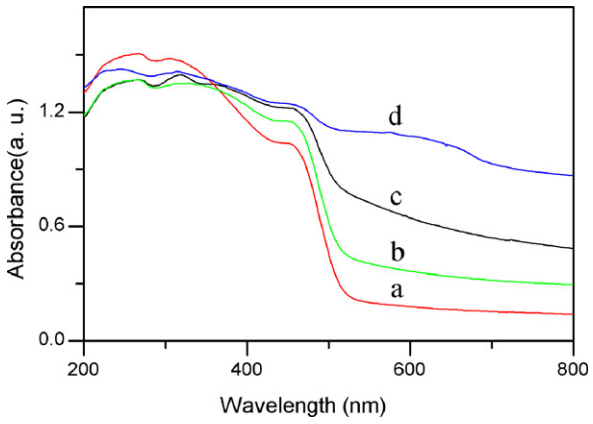

Fig. 6. UV–vis diffuse reflectance spectra for the samples synthesized at 180 °C for 3 h with a different addition of pyridine: (a) 0 mL, (b) 1 mL, (c) 2 mL and (d) 3 mL.

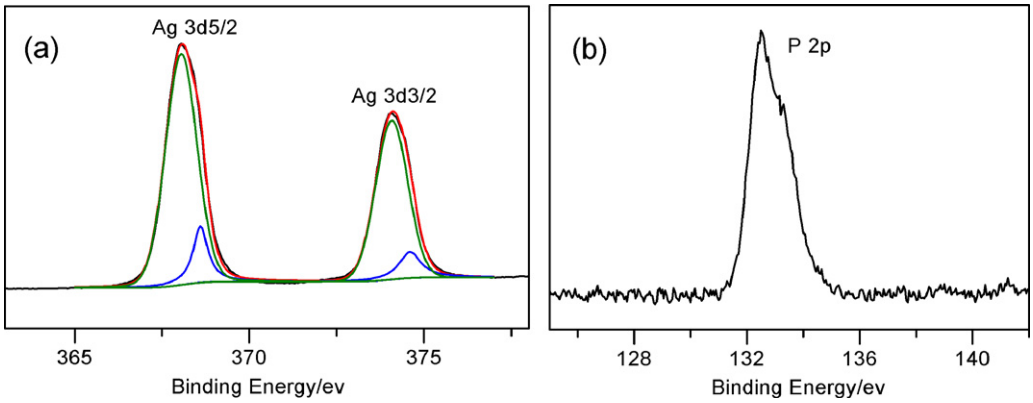

Fig. 7. XPS spectra of (a) Ag 3d and (b) P 2p for Ag/Ag_3PO_4 composite synthesized at 180 °C for 3 h with 3 mL pyridine assisted.

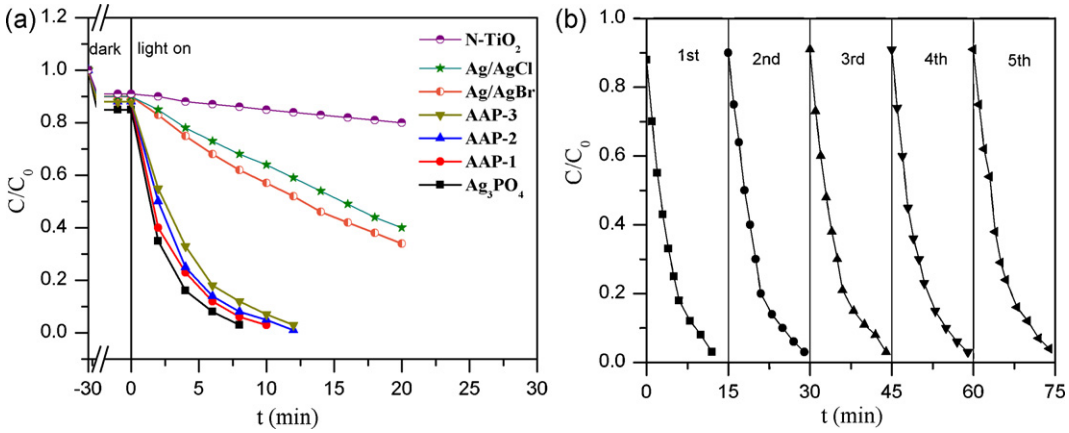

Fig. 8. (a) Photocatalytic degradation of MO with various powder samples, (b) the cycling runs of Ag/Ag_3PO_4 (AAP-3) composite for the photodegradation of MO.

at 374.6, 374.08 eV and 368.6, 368.05 eV, respectively. According to the results reported by Zhang et al. [32], the peaks at 374.6 and 368.6 eV can be attributed to Ag^0, whereas the peaks at 374.08 and 368.05 eV are attributed to Ag^+ ions in Ag_3PO_4. The calculated contents of Ag^0 and Ag^+ are 5.95 mol% and 31.7 mol%, respectively. The binding energy of P 2p coming from the Ag_3PO_4 is 132.5 eV (Fig. 7b) and the calculated amount of surface P is 12.73 mol%.

3.2. Photocatalytic activity

Fig. 8a shows the visible-light photocatalytic activity of the Ag/Ag_3PO_4 composite synthesized at 180 °C in the presence of 3 mL of pyridine. Prior to irradiation, the MO solution containing the catalyst was kept in the dark for 30 min to obtain an equilibrium adsorption state. The average rate of the MO dye

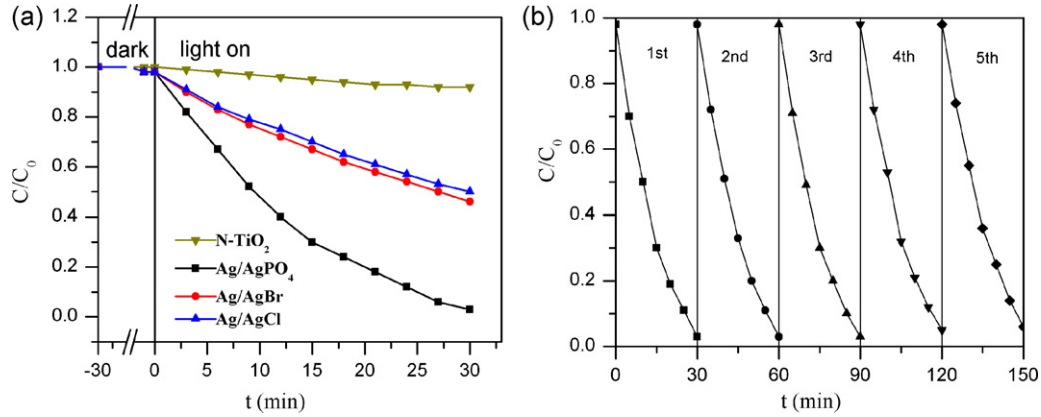

Fig. 9. (a) Photocatalytic degradation of phenol in the presence of powder samples, (b) cycling runs in the photodegradation of phenol in the presence of Ag/Ag_3PO_4 (AAP-3) composite.

decomposition over Ag_3PO_4, AAP-1, AAP-2, and AAP-3 is estimated to be about 0.248 mg min^{-1}, 0.215 mg min^{-1}, 0.182 mg min^{-1}, and 0.167 mg min^{-1}, which reveal that decomposition efficiency of Ag/Ag_3PO_4 to MO dye is slightly lower than that of Ag_3PO_4. This result of effect of loading amount of Ag on the photocatalytic activity of $Ag/AgPO_4$ is consistent with our former findings [33].

For comparison, the photocatalytic activities of the typical N-TiO_2, Ag/AgBr and Ag/AgCl were also tested under the identical experimental conditions. The absorption percentage of MO on the Ag/Ag_3PO_4 (AAP-3, S_{BET} = 0.8 m^2 g^{-1}), Ag/AgBr (S_{BET} = 0.85 m^2 g^{-1}), Ag/AgCl (S_{BET} = 0.9 m^2 g^{-1}) and N-TiO_2 (S_{BET} = 4.7 m^2 g^{-1}) was about 12%, 10%, 10%, 9%, respectively. For all the photocatalysts, the concentration of MO is steadily decreased with increasing irradiation time. The average decomposition rate of Ag/Ag_3PO_4 (AAP-3, 0.146 mg min^{-1}) is higher than that of Ag/AgBr (0.057 mg min^{-1}), Ag/AgCl (0.050 mg min^{-1}) and N-TiO_2 (0.011 mg min^{-1}). Therefore, it is obvious that the Ag/Ag_3PO_4 (AAP-3) photocatalyst shows the highest photocatalytic efficiency for the decomposition of MO dye, which is about three times that of Ag/AgBr and Ag/AgCl and is dozens of times that of N-TiO_2. The possible reason for the high performance of Ag/Ag_3PO_4 could be related to a high position of the valence band and inductive effect of the PO_4^{3-} that promotes the efficient separation of photogenerated electrons and holes [34]. To further investigate the performance stability of the prepared Ag/Ag_3PO_4 (AAP-3), the cycling degradation of MO experiments were carried out, as shown in Fig. 8b. It was found that the Ag/Ag_3PO_4 (AAP-3) still maintains a high photocatalytic activity even after 5-time repeated reaction. Furthermore, the corresponding XRD results suggest that there is a negligible change about the phase structure of Ag/Ag_3PO_4 (AAP-3) sample before and after repeated photocatalytic reactions, indicating that the prepared Ag/Ag_3PO_4 (AAP-3) photocatalysts can work as a stable and efficient visible-light photocatalyst (Fig. 10b).

The photocatalytic performance of Ag/Ag_3PO_4 (AAP-3) was also evaluated by the photodegradation of phenol aqueous solution under visible light irradiation, as shown in Fig. 9a. Prior to irradiation, it is clear that almost no phenol is adsorbed on the surface of Ag/Ag_3PO_4 (AAP-3) photocatalyst. When the light was turn on, the Ag/Ag_3PO_4 composite shows a higher photocatalytic activity for the decomposition of phenol compared with Ag/AgBr, Ag/AgCl and N-TiO_2 photocatalyst. Moreover, the Ag/Ag_3PO_4 (AAP-3) composite is also demonstrated to be a stable (Fig. 10c) and efficient visible-light photocatalyst (Fig. 9b).

It is interesting and important to consider how Ag/Ag_3PO_4 can act as a stable and efficient photocatalyst under visible-light irradiation. In the Ag/Ag_3PO_4 system, photons from the visible light irradiation could be absorbed by Ag_3PO_4 and Ag^0, and the photogenerated electrons and holes were produced. The LSPR produced by the collective oscillations of surface electrons on Ag nanoparticles could induce enhancement of the local inner electromagnetic field. The electrons and holes generated by the Ag_3PO_4 could be separated efficiently with the help of the local electromagnetic field. Due to the local electromagnetic field and excellent conductivity of silver nanoparticles, the electron can be transferred quickly and induced away from Ag_3PO_4 as far as possible, instead of remain in the Ag^+ ions of the Ag_3PO_4 lattice. Electrons generated by Ag_3PO_4 would transfer to Ag^0 nanoparticles and then reduce the present molecular oxygen to form the O_2^- active species [35]. Nevertheless, photogenerated holes tend to remain on the surface of Ag_3PO_4 due to that PO_4^{3-} ions have large negative charge which prefers to attract holes and repel electrons. Meanwhile, PO_4^{3-} ions on the surface of Ag_3PO_4 have strong bonding ability with H_2O. As a result, H_2O could be adsorbed on surface easily and then be oxidized by the holes to OH·, which eventually oxidizes dye and phenol to carbon dioxide (Fig. 11). So the Ag/Ag_3PO_4 composite could show efficient activity and remain stable without deterioration. The similar research result was also found on Ag_2O [36] and AgBr [20] photosensitive materials. Those results strongly support that the structure stability of Ag-based materials can be markedly enhanced by metallic Ag.

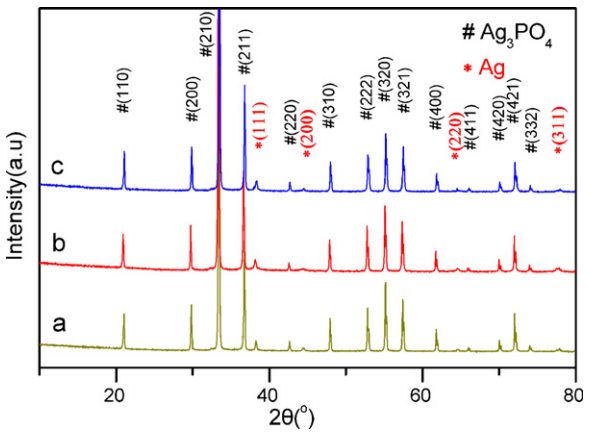

Fig. 10. XRD patterns of (a) as-prepared Ag/Ag_3PO_4 (AAP-3) composite, (b) Ag/Ag_3PO_4 (AAP-3) after the 5th cycling photodegradation of MO and (c) Ag/Ag_3PO_4 (AAP-3) after the 5th cycling photodegradation of phenol under visible light irradiation.

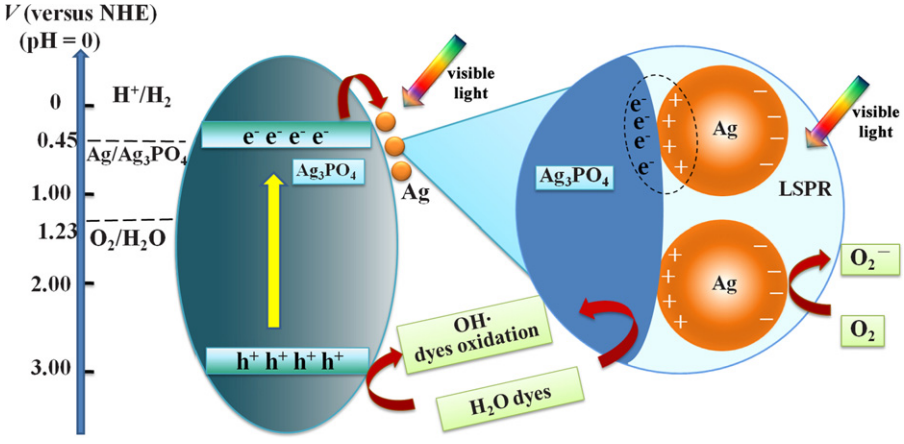

Fig. 11. Schematic model of the photocatalytic mechanism for Ag/Ag_3PO_4 composite.

4. Conclusions

A highly efficient and stable Ag/Ag_3PO_4 photocatalyst was prepared by one-pot hydrothermal method assisted by pyridine. In the reaction system, pyridine not only plays a coordination agent role for Ag^+, but also acts as a reducing reagent to reduce partial Ag^+ in Ag_3PO_4 to metallic Ag. The Ag/Ag_3PO_4 composite was efficient and stable for the degradation of MO and phenol under visible light irradiation. It is a promising candidate for the removal of hazardous organic materials from wastewater. In addition, the synthesis method of this material would be application in preparation of other effective Ag/semiconductor composites.

References

[1] A.L. Linsebigler, G. Lu, J.T. Yates, Chem. Rev. 95 (1995) 735–758.
[2] Y. Wang, C. Feng, M. Zhang, J. Yang, Z. Zhang, Appl. Catal. B 100 (2010) 84–90.
[3] I.K. Konstantinou, T.A. Albanis, Appl. Catal. B 49 (2004) 1–14.
[4] H.G. Kim, D.W. Hwang, J.S. Lee, J. Am. Chem. Soc. 126 (2004) 8912–8913.
[5] B. Zhou, X. Zhao, H. Liu, J. Qu, C.P. Huang, Appl. Catal. B 99 (2010) 214–221.
[6] S. Sun, W. Wang, J. Xu, L. Wang, Z. Zhang, Appl. Catal. B 106 (2011) 559–564.
[7] X. Xu, R. Lu, X. Zhao, S. Xu, X. Lei, F. Zhang, D.G. Evans, Appl. Catal. B 102 (2011) 147–156.
[8] U. Sulaeman, S. Yin, T. Sato, Appl. Catal. B 105 (2011) 206–210.
[9] Z. Yi, J. Ye, N. Kikugawa, T. Kako, S. Ouyang, H. Stuart-Williams, H. Yang, J. Cao, W. Luo, Z. Li, Y. Liu, R.L. Withers, Nat. Mater. 9 (2010) 559–564.
[10] Y. Bi, S. Ouyang, N. Umezawa, J. Cao, J. Ye, J. Am. Chem. Soc. 133 (2011) 6490–6492.
[11] X. Ma, B. Lu, D. Li, R. Shi, C. Pan, Y. Zhu, J. Phys. Chem. C 115 (2011) 4680–4687.
[12] A.J. Bard, R. Parsons, J. Jordan, Standard Potentials in Aqueous Solution, CRC press, 1985.
[13] K. Awazu, M. Fujimaki, C. Rockstuhl, J. Tominaga, H. Murakami, Y. Ohki, N. Yoshida, T. Watanabe, J. Am. Chem. Soc. 130 (2008) 1676–1680.
[14] P. Wang, B. Huang, X. Qin, X. Zhang, Y. Dai, J. Wei, M.-H. Whangbo, Angew. Chem. 120 (2008) 8049–8051.
[15] X. Chen, H.-Y. Zhu, J.-C. Zhao, Z.-F. Zheng, X.-P. Gao, Angew. Chem. Int. Ed. 47 (2008) 5353–5356.
[16] P. Wang, B. Huang, Z. Lou, X. Zhang, X. Qin, Y. Dai, Z. Zheng, X. Wang, Chem.: Eur. J. 16 (2009) 538–544.
[17] C. An, S. Peng, Y. Sun, Adv. Mater. 22 (2010) 2570–2574.
[18] Y. Tang, V.P. Subramaniam, T.H. Lau, Y. Lai, D. Gong, P.D. Kanhere, Y.H. Cheng, Z. Chen, Z. Dong, Appl. Catal. B 106 (2011) 577–585.
[19] Z. Yan, G. Compagnini, D.B. Chrisey, J. Phys. Chem. C 115 (2010) 5058–5062.
[20] P. Wang, B. Huang, X. Zhang, X. Qin, H. Jin, Y. Dai, Z. Wang, J. Wei, J. Zhan, S. Wang, J. Wang, M.-H. Whangbo, Chem.: Eur. J. 15 (2009) 1821–1824.
[21] L. Kuai, B. Geng, X. Chen, Y. Zhao, Y. Luo, Langmuir 26 (2010) 18723–18727.
[22] C. Hu, T. Peng, X. Hu, Y. Nie, X. Zhou, J. Qu, H. He, J. Am. Chem. Soc. 132 (2010) 857–862.
[23] M.R. Elahifard, S. Rahimnejad, S. Haghighi, M.R. Gholami, J. Am. Chem. Soc. 129 (2007) 9552–9553.
[24] Y. Zhang, Z.-R. Tang, X. Fu, Y.-J. Xu, Appl. Catal. B 106 (2011) 445–452.
[25] L. Zhang, K.-H. Wong, Z. Chen, J.C. Yu, J. Zhao, C. Hu, C.-Y. Chan, P.-K. Wong, Appl. Catal. A 363 (2009) 221–229.
[26] Y. Nakajima, Q. Jin, H. Tada, Electrochem. Commun. 10 (2008) 1132–1135.
[27] J.-F. Guo, B. Ma, A. Yin, K. Fan, W.-L. Dai, Appl. Catal. B 101 (2011) 580–586.
[28] H.N. Ng, C. Calvo, R. Faggiani, Acta Crystallogr., Sect. B 34 (1978) 898–899.
[29] J.-M. Song, Y.-Z. Lin, H.-B. Yao, F.-J. Fan, X.-G. Li, S.-H. Yu, ACS Nano 3 (2009) 653–660.
[30] S. Chakraborty, O. Dopfer, ChemPhysChem 12 (2011) 1999–2008.
[31] E.V. Potapkina, A.S. Denisova, L.A. Myund, A.A. Makarov, E.M. Dem'yanchuk, J. Mol. Struct. 996 (2011) 128–134.
[32] H. Zhang, G. Wang, D. Chen, X. Lv, J. Li, Chem. Mater. 20 (2008) 6543–6549.
[33] Y. Liu, L. Fang, H. Lu, L. Liu, H. Wang, C. Hu, Catal. Commun. 17 (2012) 200–204.
[34] C. Pan, Y. Zhu, Environ. Sci. Technol. 44 (2010) 5570–5574.
[35] J. Yu, G. Dai, B. Huang, J. Phys. Chem. C 113 (2009) 16394–16401.
[36] X. Wang, S. Li, H. Yu, J. Yu, S. Liu, Chem.: Eur. J. 17 (2011) 7777–7780.